ELSEVIER
(https://www.elsevier.com/)

Home (https://www.elsevier.com/) › Journals (https://www.elsevier.com/catalog?producttype=... SEARCH MENU()
› Energy (https://www.journals.elsevier.com:443/energy)

(https://www.facebook.com/elsevierenergy) (//twitter.com/elsevierenergy) (/energy/rss) (https://www.elsevier.com/PreferenceCentre)

(https://www.sciencedirect.com/science/journal/03605442)

ISSN: 0360-5442

Energy

The International Journal

› Supports Open Access (http://www.elsevier.com/journals/energy/0360-5442/open-access-options)

Editor-in-Chief: Henrik Lund (https://www.journals.elsevier.com:443/energy/editorial-board/henrik-lund)

› View Editorial Board (https://www.journals.elsevier.com:443/energy/editorial-board)

Submit Your Paper

View Articles (https://www.sciencedirect.com/science/journal/03605442)

Guide for Authors

Abstracting/ Indexing (http://www.elsevier.com/journals/energy/0360-5442/abstracting-indexing)

ELSEVIER
(https://www.elsevier.com/)

Home (https://www.elsevier.com/) › Journals (https://www.elsevier.com/catalog?producttype=... SEARCH MENU()
› Energy (https://www.journals.elsevier.com:443/energy)
› Editorial Board (https://www.journals.elsevier.com:443/energy/editorial-board)

Submit Your Paper

View Articles (https://www.sciencedirect.com/science/journal/03605442)

Guide for Authors

Abstracting/ Indexing (http://www.elsevier.com/journals/energy/0360-5442/abstracting-indexing)

Track Your Paper

Order Journal (https://www.elsevier.com/journals/institutional/energy/0360-5442)

Journal Metrics ()

CiteScore: **5.17**

More about CiteScore (https://www.scopus.com/sourceid/29348)

Impact Factor: **4.520**

5-Year Impact Factor: **5.182**

Source Normalized Impact per Paper (SNIP): **1.798**

SCImago Journal Rank (SJR): **1.999**

› View More on Journal Insights (http://journalinsights.elsevier.com/journals/0360-5442)

Article Enrichments

› AudioSlides (https://www.elsevier.com/authors/author-services/enrichments/audioslides)

› Data in Brief co-submission (https://www.elsevier.com/authors/author-services/research-elements/data-articles/DIB-co-submission)

- Interactive Plot Viewer (https://www.elsevier.com/authors/author-services/enrichments/iplots)

Related Links ()

- Author Stats (https://www.mendeley.com/stats/welcome?dgcid=journals_referral_related-links) ⓘ
- Publishing Campus (https://www.publishingcampus.elsevier.com)
- Author Services (https://www.elsevier.com/authors/author-services)

Energy Editorial Board

Editor-in-Chief

Deputy Editors-in-Chief

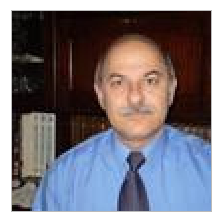

Subject Editors

Jesse Thé (https://www.journals.elsevier.com:443/energy/editorial-board/jesse-the)
University of Waterloo, Waterloo, Ontario, Canada

Petar Varbanov (https://www.journals.elsevier.com:443/energy/editorial-board/petar-varbanov)
Pázmány Péter Catholic University, Budapest, Hungary

Assistant Editors

Rafaela Agathokleous

Cyprus University of Technology, Limassol, Cyprus
Email Rafaela Agathokleous (https://www.journals.elsevier.com:443/energy/editorial-board/rafaela-agathokleous)

Pernille S. Andersen

Aalborg University, Aalborg, Denmark
Email Pernille S. Andersen (https://www.journals.elsevier.com:443/energy/editorial-board/pernille-s-andersen)

Lars Grundahl

Aalborg University, Denmark
Email Lars Grundahl (https://www.journals.elsevier.com:443/energy/editorial-board/lars-grundahl)

Weili Luo

Shanghai Jiaotong University, Shanghai, China
Email Weili Luo (https://www.journals.elsevier.com:443/energy/editorial-board/weili-luo)

Mette Reiche Sørensen

Aalborg University, Aalborg, Denmark
Email Mette Reiche Sørensen (https://www.journals.elsevier.com:443/energy/editorial-

board/mette-reiche-srensen)

Term Ending 2017

Linda Barelli (https://www.journals.elsevier.com:443/energy/editorial-board/linda-barelli)
University of Perugia, Perugia, Italy

Robert Boehm

University of Nevada, Las Vegas, Nevada, USA

Zeljko Bogdan (https://www.journals.elsevier.com:443/energy/editorial-board/zeljko-bogdan)
Sveučilišta u Zagrebu, Zagreb, Croatia

Maria de Graca Carvalho

Universidade de Lisboa, São João De Deus, Lisboa, Portugal

Christos Frangopoulos (https://www.journals.elsevier.com:443/energy/editorial-board/christos-frangopoulos)
National Technical University of Athens (NTUA), Athens, Greece

Mejdi Jeguirim (https://www.journals.elsevier.com:443/energy/editorial-board/mejdi-jeguirim)

Term Ending 2018

Fengqi Zhou

Shanghai Academy of Social Sciences, Shanghai, China

Term Ending 2019

Naim Hamdia Afgan

Universidade de Lisboa, Lisbon, Portugal

Mohammad A. Al-Nimr (https://www.journals.elsevier.com:443/energy/editorial-board/mohammad-a-al-nimr)
Jordan University of Science and Technology, Irbid, Jordan

Beng Wah Ang

National University of Singapore, Singapore, Singapore

Giorgio Besagni

Politecnico di Milano, Milano, Italy

S.H. Chan (https://www.journals.elsevier.com:443/energy/editorial-board/sh-chan)
Yuan Ze University, Taoyuan, Taiwan, ROC

Silvio De Oliveira, Jr (https://www.journals.elsevier.com:443/energy/editorial-board/silvio-de-oliveira-jr)

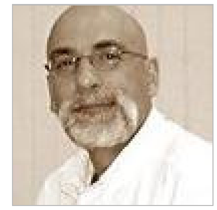

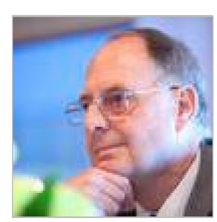

Qiang Liao

Chongqing University, Chongqing, China

Tyrone Lin

National Dong Hwa University, Shou-Feng, Hualien, Taiwan

Noam Lior (https://www.journals.elsevier.com:443/energy/editorial-board/noam-lior)

University of Pennsylvania, Philadelphia, Pennsylvania, USA

Adel Mellit

University of Jijel, Jijel, Algeria

Michael Moran

The Ohio State University, Columbus, Ohio, USA

Luis Serra (https://www.journals.elsevier.com:443/energy/editorial-board/luis-serra)

Universidad de Zaragoza, Zaragoza, Spain

Vladimir Stevanovic

Vladimir Stevanovic

University of Belgrade, Belgrade, Serbia

Arnaldo Walter

Universidade Estadual de Campinas (UNICAMP), Sao Paulo, Brazil

Chi-Keung Woo

Chi-Keung Woo

Hong Kong Institute of Education, Hong Kong

Jinyue Yan (https://www.journals.elsevier.com:443/energy/editorial-board/jinyue-yan)
KTH Royal Institute of Technology, Stockholm, Sweden

Book Review Panel

Henrik Lund (https://www.journals.elsevier.com:443/energy/editorial-board/henrik-lund)

Soteris Kalogirou (https://www.journals.elsevier.com:443/energy/editorial-board/soteris-kalogirou)

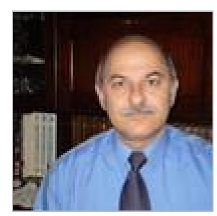

Krzysztof Ptasinski

John Twidell

Energy

Readers
View Articles (https://www.sciencedirect.com/science/journal/03605442)
Volume/ Issue Alert (http://www.sciencedirect.com/science/alerts)

Authors (http://www.elsevier.com/authors/home)
Author Information Pack (http://www.elsevier.com/journals/energy/0360-5442?generatepdf=true)
Submit Your Paper (http://ees.elsevier.com/egy/)
Track Your Paper (http://help.elsevier.com/app/answers/detail/a_id/89/p/8045/)
Early Career Resources (http://www.elsevier.com/early-career-researchers/training-and-workshops)
Webshop (http://webshop.elsevier.com/)
Customer Service (https://service.elsevier.com)

Librarians (http://www.elsevier.com/librarians/home)
Ordering Information and Dispatch Dates (http://www.elsevier.com/journals/energy/0360-5442/order-journal)
Abstracting/ Indexing (http://www.elsevier.com/journals/energy/0360-5442/abstracting-indexing)

Editors (http://www.elsevier.com/editors/home)
Publishing Ethics Resource Kit (http://www.elsevier.com/editors/perk)
Support (http://service.elsevier.com/app/answers/list/supporthub/publishing/p/10593/)
Guest Editors (http://www.elsevier.com/editors/guest-editors)

Reviewers (http://www.elsevier.com/reviewers/home)
Reviewer Guidelines (http://www.elsevier.com/reviewersguidelines)
Log in as Reviewer (http://ees.elsevier.com/egy/login.asp)

Journals Books pengguna ristekdikti65

Search all fields | Author name | --This Journal/Book-- | Volume | Issue | Page | Advanced search

Energy

Supports Open Access | About this Journal | Sample Issue Online | Submit your Article

Incorporating **Exergy, An International Journal**;

Get new article feed
Get new Open Access article feed
Subscribe to new volume alerts
Add to Favorites

Energy
Volume 134, Pages 1-1140 (1 September 2017)

Articles **1 - 96**

View issue

< Previous vol/iss | Next vol/iss >

Download PDFs | Export | **All access types**

Full Length Articles

Highlights

- Performance test platform for high speed micro radial turbine was set up.
- Operating and overall performance test of micro radial turbine was carried out.
- Rotational speed of micro radial turbine has achieved at 359,900 r/min.
- Feasibility of micro radial turbine with 10 mm diameter has partly been proven.
- Problems and solutions can be referenced for other micro turbine designer.

Highlights

- AAEM role on biomass pyrolysis was investigated to answer to the several open queries.
- Salts impregnation by ionic exchange mechanism preserves the biomass structure.
- AAEM affects both the chars morphology and the pyrolysis products distribution.
- Alkaline metals promote the decomposition of cellulose and hemicellulose polymers.
- Alkaline earth metals inhibit the hemicellulose thermal degradation.

Optimization of transesterification process for *Ceiba pentandra* oil: A comparative study between kernel-based extreme learning machine and artificial neural networks Original Research Article
Pages 24-34
F. Kusumo, A.S. Silitonga, H.H. Masjuki, Hwai Chyuan Ong, J. Siswantoro, T.M.I. Mahlia
Abstract | Close research highlights | PDF (1801 K) | View PDF

Highlights

- C. *pentandra* oil was explored as the potential feedstock for biodiesel production.
- Kernel extreme learning machine and artificial neural network were used for modelling.
- Kernel-based extreme learning machine was superior to artificial neural network.
- The predicted methyl ester yield by kernel extreme learning machine was 99.8%.
- The properties of biodiesel produced met ASTM D6751 and EN 14214 standards.

Experimental and modeling investigation of an organic Rankine cycle system based on the scroll expander Original Research Article
Pages 35-49
Zheng Miao, Jinliang Xu, Kai Zhang
Abstract | Close research highlights | PDF (3112 K) | View PDF

Highlights

- An ORC model is developed to analyze the mismatch among different components.
- Effects of non-condensable gas and environment conditions are considered.
- System performance can be significantly improved after the optimization.
- Expander built-in volume ratio and backpressure are concerns of cycle design.
- The environment temperature and humidity strongly affect the ORC performance.

Energy efficiency of perennial herbaceous crops production depending on the type of digestate and mineral fertilizers Original Research Article
Pages 50-60
Mariusz J. Stolarski, Michał Krzyżaniak, Kazimierz Warmiński, Józef Tworkowski, Stefan Szczukowski, Ewelina Olba–Zięty, Janusz Gołaszewski
Abstract | Close research highlights | PDF (551 K) | View PDF

Highlights

- The total energy input ranged widely from 2.83 to 59.08 GJ ha^{-1}.
- The highest energy gain was for *Helianthus salicifolius* (139.6 GJ ha^{-1} $year^{-1}$).
- Better energy efficiency ratios for all species were at the control plots.
- The highest energy ratio (19.1) was obtained for *Helianthus salicifolius*.
- Fertilisers resulted in lower energy efficiency of crops production.

Thermal investigation of a PEM fuel cell with cooling flow field Original Research Article

Highlights

- This paper provides a new way to study temperature distribution of PEM catalyst.
- Both electrochemistry and cooling flow field effect were simultaneously simulated.
- The study was proposed by heat flux contours & index of uniformity temperature (IUT).
- IUT was 24% improved in serpentine cooling channel than parallel one.

Highlights

- Microwave hydrothermal carbonization can convert human biowaste to solid fuel chars.
- Physicochemical, structural, energetic and combustion properties of chars are enhanced.
- Higher heating value (HHV) of chars recovered increased by up to 41.5%.
- HHV of chars – up to 25.6 MJ/kg – is greater than that of low-ranking coals/fuels.
- Processing human biowaste into solid fuel is promising for energy applications.

Highlights

- A cluster analysis strategy was developed to identify building typical load profiles.
- Pearson correlation coefficient-based distance was used as the dissimilarity measure.
- Differences between this strategy and ED-based approaches were demonstrated.
- Information discovered matched with the practical findings from building operation.

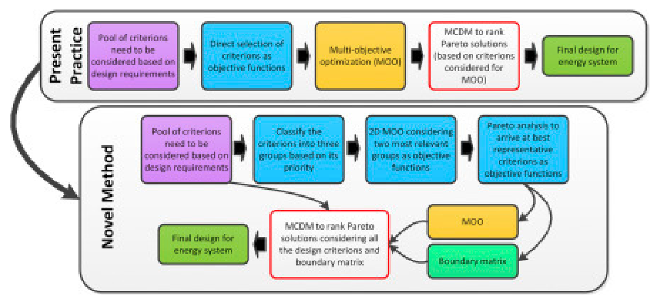

Online fault detection and the economic analysis of grid-connected photovoltaic systems Original Research Article
Pages 121-135
Siva Ramakrishna Madeti, S.N. Singh
Abstract | Close research highlights | PDF (5249 K) | View PDF

Highlights

- A monitoring system with optimized voltage sensor locations is developed.
- A low-cost online fault detection technique is presented for GCPV system.
- The procedure can detect and locate the fault to modular level.
- Economic analysis shown for the proposed fault detection technique.

Design of explicit models for estimating efficiency characteristics of microbial fuel cells Original Research Article
Pages 136-156
A. Garg, Jasmine Siu Lee Lam
Abstract | Close research highlights | PDF (7262 K) | View PDF

Highlights

- Need for modelling of microbial fuel cell by optimization methods is addressed.
- This study models efficiency characteristics of fuel cells.
- Power density and voltage output of fuel cells are analysed.
- Genetic programming models perform better than multi-adaptive regression splines.
- Sensitivity/parametric analysis provides relationships between fuel cell parameters.

A cost-emission framework for hub energy system under demand response program Original Research Article
Pages 157-166
Majid Majidi, Sayyad Nojavan, Kazem Zare
Abstract | Close research highlights | PDF (2327 K) | View PDF

Highlights

- An economic-environmental model is proposed for operation of energy hub system.
- Weighted-sum technique has been employed to solve the proposed multi-objective model.
- Min-max fuzzy method has been utilized to select the best compromise solution.
- Demand response program is used to flatten load curve and minimize operation cost.

Analytical solution for the study of time lag and decrement factor for building walls in climate of Iran Original Research Article
Pages 167-180
Reza Fathipour, Amin Hadidi
Abstract | Close research highlights | PDF (2469 K) | View PDF

Highlights

- Analytical method is proposed to determinate of decrement factor and time lag.
- Decrement factor and time lag determined for climate of Iran.
- Effects of combined convection and radiation heat transfer coefficients.
- Effect of insulation in walls studied on time lag and the decrement factor.

Highlights

- A field-scale numerical model to simulate CO_2-EOR in tight oil is developed.
- Comparison of CO_2 Huff-n-Puff and flooding scenarios in the Bakken formation is performed.
- Sensitivity studies are performed to quantify the key parameters.
- Fracture half-length and permeability are important in designing CO_2-EOR process.

Highlights

- Energy efficient distillation technologies are applied on EB/SM column.
- Innovative retrofit scenarios with attractive payback periods are proposed.
- Significant reduction in energy consumption as well as total annualized cost.
- Optimization of advanced distillation schemes through sensitivity analysis.

Highlights

- A HEM approach is presented for decreasing the energy cost in a smart house.
- The HEM approach considers both load and source side dynamics with a 5-min time step.
- Consumer preferences, load demand, battery SOC and electricity tariff are taken into account.
- Expected renewable power generations are also considered in the scheduling process.
- The effectiveness of the proposed HEM approach is experimentally validated.

Highlights

- Ambient temperature is affects the power generating and the efficiency of power plant.

- The ambient temperature has an impact on the levelised cost of electricity.
- The design of power plant requires flexibility to operate with and without capture.
- LP steam turbine capable to operate with capture off line but condenser with capture.

Highlights

- Enhancing the cetane number additive of DTBP to biodiesel as CI engine fuel.
- Coated engine fuelled by biodiesel with DTBP additive.
- Significant increase in brake thermal efficiency.
- The brake fuel consumption also decreased significantly.
- Significant effect in reduction of HC, CO, NOx and smoke emissions.

Highlights

- A new cost allocation method based on energy level has been proposed.
- The continuous cost change within each component is considered in this method.
- The unit energy cost is adopted to evaluate the products.
- The cost allocation results of different methods are presented and compared.

Highlights

- Monochromatic light absorption in a multi-junction photovoltaic cell is formulated.
- Iterative algorithm was established to calculate the laser energy depositions distribution.
- Temperature characteristics of the film photovoltaic cell are analyzed by FEM.

Highlights

- Grid-connected and off-grid PV systems are examined by techno-economic evaluation.
- The levelized cost of energy (LCOE) of PV systems is calculated for five regions.
- The grid parity of PV power generation in China is estimated using learning curves.
- Grid parity varies across regions based on solar radiation and electricity prices.

- Policy implications are given to promote market deployment of China's PV industry.

Highlights

- Swash plate is used to adjust the blade pitch angle.
- Aerodynamic force of FOWT is investigated in the diagonal inflow wind condition.
- Power and thrust coefficients were almost constant regardless of the amplitude of the periodic change.
- Cyclic pitch control showed the possibility of reducing the load vibrations acting on the wind turbine.
- Load change on yaw system can be controlled by cyclic pitch control.

Highlights

- Energy harvesting of half vehicle model for harmonic and random road excitations.
- The effect of road frequency, velocity and road amplitude on energy harvesting.
- Studying the energy harvesting of vehicle bounce and pitch motions (4DOF system).
- For the random excitation, smooth highway and highway with gravels were studied.
- Pitch motion of vehicle has a considerable effect on the potential harvested power.

Highlights

- Socio-economic analysis of the usage of biogas and biomethane in the energy system.
- Natural gas and biomethane technologies are combined in Balmorel.
- A common target for biogas and biomethane is added to Balmorel.
- Socio-economic analysis of biogas related to several CO_2-externality cost estimates.
- The CO_2-cost has to be very high in order for biogas to be worthwhile.

Highlights

- Co-pyrolysis of biomass and DOA does not show synergetic effect on the char yield.
- DOA melt and stuck to biomass surface causes the char an obvious

agglomeration.

- Synergetic effect is observed during gasification of the co-pyrolysis chars.
- Co-gasification of DOA and biomass is a good choice for disposing DOA.

Estimating the benefits of vehicle-to-home in islands: The case of the Canary Islands Original Research Article
Pages 311-322
A. Colmenar-Santos, Carlos de Palacio-Rodriguez, Enrique Rosales-Asensio, David Borge-Diez
Abstract | Close graphical abstract | Research highlights | PDF (1906 K) | View PDF

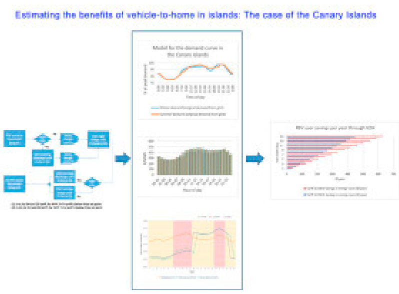

Dynamic modeling of gravity energy storage coupled with a PV energy plant Original Research Article
Pages 323-335
Asmae Berrada, Khalid Loudiyi, Raquel Garde
Abstract | Close research highlights | PDF (2727 K) | View PDF

Highlights

- Dynamic behavior of gravity storage is analyzed.
- Operation modeling of a gravity energy storage coupled with a PV plant.
- Validation of the model by a case study.
- Storage system response to load variation is studied.

Life cycle building impact of a Middle Eastern residential neighborhood Original Research Article
Pages 336-348
Catherine De Wolf, Carlos Cerezo, Zainab Murtadhawi, Ali Hajiah, Adil Al Mumin, John Ochsendorf, Christoph Reinhart
Abstract | Close research highlights | PDF (2336 K) | View PDF

Highlights

- Embodied and operational carbon simulation of buildings.
- Urban modeling simulation methodology on a neighborhood scale.
- Middle Eastern residential neighborhood case study: Al-Qādisiyyah.
- Recommendations/strategies to lower environmental impact of Middle Eastern cities.

A new optimal power flow approach for wind energy integrated power systems Original Research Article
Pages 349-359
Shima Rahmani, Nima Amjady
Abstract | Close research highlights | PDF (902 K) | View PDF

Highlights

- A new scenario generation approach is presented.
- A new wind power integrated optimal power model is proposed.
- A new out-of-sample analysis is presented.
- The effectiveness of the proposed model is extensively illustrated.

Highlights

- Multi criteria decision approach is implemented for energy performance prioritization.
- Nusselt number and friction factor are evaluated at different control factor combinations.
- The Entropy method is powerful tool for weight determination of control factors.

Highlights

- The off-design performance of a Balanced Hybrid Rankine-Brayton cycle is analyzed.
- The cycle is integrated in a STPP with parabolic trough collectors (HTF at 670 K).
- Working fluid selection is key issue to guarantee suitable off-design operation.
- Several organic fluids show a suitable performance, even under stream conditions.
- Propane is a good option with efficiencies from 41.4 to 30.2% (yearly operation).

Highlights

- A solar dryer system was developed to determine the drying kinetics of apple.
- A mathematical model is presented to predict the drying curve in drying process.
- Experiments in the solar dryer are used to validate the model.
- Thermal energy storage was used to ensure the continuity of the drying process.

Highlights

- To evaluate inter-temporal efficiency based on OECD countries and China.
- The effects of the undesirable output and carry-over variable in order to rank the OECD countries and China.

- These 27 countries should thus increase the number of energy stock to improve their efficiency.

Highlights

- The efficiency optimal control method of micro gas turbine(MGT) is proposed.
- The MGT efficiency of four operation modes is studied.
- The existence of the efficiency optimal operation point by changing speed is verified.
- Efficiency of the efficiency optimal mode and the constant speed mode is compared.
- The variable speed mode of regenerative cycle is optimal and more obvious effect with light load.

Highlights

- Bendable polymer electrolyte fuel cell was fabricated using silver nanowires.
- Effect of assembly pressure on bendable fuel cell was investigated experimentally.
- Causes of performance loss by bending in bendable fuel cell were figured out.
- Simulation model of bendable fuel cell was established based on experimental data.
- Simulation model predicts performances of other bendable fuel cells in literatures.

Highlights

- Boot injection dynamics is analyzed on the basis of tests at the hydraulic rig.
- Continuous injection rate shaping schedules are implemented in a *PCCI* type engine.
- The effects of the boot injection parameters on emissions, combustion noise and fuel consumption are assessed.

Highlights

- An optimal sizing method for combined cooling, heat and power projects is proposed.
- Combined cooling, heat and power projects at district level still require support.
- Public support has to be specifically designed per project.

Highlights

- The continuous- and batch-types CLAS processes are developed in Aspen Plus®.
- The integration of CLAS and OCM becomes the stand-alone oxygen production system.
- The oxygen production cost by the Design 2 is cheaper than it by the conventional design.
- A suitable combination of oxygen carriers and inert binder ensures near-zero CO_2 emissions.

Highlights

- Proactive integration of EVs could alleviate future grid problems.
- A proper regulatory framework to allow EV distribution grid services is missing.
- Definition of theoretical and practical flexibility attributes is provided.
- Identification of both technological and non-technological barriers.
- Policy recommendations for lowering the barriers are drawn.

Highlights

- Optimal transmission expansion allows highly renewable systems at current cost levels.
- Restricting transmission expansion leads to a non-linear cost increase by up to 30%.
- A relatively moderate amount of transmission already locks in most of the benefits.
- Wind generation is mostly smoothed by transmission, solar PV by shortterm storage.

Highlights

- Effects of turbulence intensity and wind shear were compared by field experiments.

- An ultrasonic current meter (SAT-550) was used for the wake measurement.
- Maximum velocity deficit in the wake was reduced with the increase of the turbulence intensity.
- As the increase of the wind shear index, the maximum velocity deficit in the wake was increased.
- Maximum velocity deficit in the wake was increased with the increase of the tip speed ratio.

Highlights

- In this work, the performances of five kinds of the carbon-centered organocatalysts have been investigated, theoretically.
- Different aspects of the proposed mechanism on the CO_2 reduction to methanol have been analyzed.
- High local nucleophilicity index of the carbon atom corresponds to low activation energy of CO_2 activation.
- NICS-XY scan was applied for investigation of the aromaticity character in the studied organocatalysts.
- A good relationship between the aromaticity and nucleophilicity character of the organocatalysts was obtained.

Highlights

- Stability and availability of China's first SPR salt caverns are investigated.
- Jintan salt mine has a good feasibility for the SPR caverns construction.
- Operating parameters are proposed to ensure the safety of SPR salt caverns.
- Many abandoned salt caverns of China can be rebuilt as the SPR caverns.
- Interlayers are beneficial for the stability of SPR caverns in Jintan bedded salt formation.

Highlights

- Exergy, economic and environmental analysis of a SOFC-GT performs.
- Optimization performs by NSGA-II and interactive fuzzy multi-objective method.
- Sensitivity analysis of change in objective functions with fuel unit cost.
- Investigation of current density changes impact on cell voltage and voltage losses.
- Studying of thermodynamic parameters changes on exergy efficiency and output power.

Highlights

- Savonius turbine suffers low efficiency problem.
- This research paper proposes a novel system of ducted nozzle configuration around Savonius rotor.
- In this study, six different duct nozzle designs had been investigated numerically.
- The ducted nozzle shields the returning blade, thus reducing the reversing torque of the turbine.
- The maximum power coefficient of the ducted nozzle turbine was increased by 78% compared to the conventional rotor.

Highlights

- New method to minimize the cost of latent heat energy storage systems is developed.
- An analytic solution for the time to melt of a PCM in a heat exchanger is developed.
- The relationships between the optimal cost and design choices are explored.

Highlights

- Benefits of energy efficiency programs for KSA new and existing buildings are evaluated.
- Optimization based analysis has been used in the analysis using a wide range of technologies.
- Significant benefits can incur form large scale building energy retrofit programs.

Highlights

- We developed a multi-criteria optimisation for wind power allocation for multiple scales.
- System friendly wind power technology outperforms standard technology.
- For both technologies, trade-offs between electricity production, human and environmental well-being, are significant.

Highlights

- The US coal fleet has large variations in plant-level LCA emissions.
- Likely large emissions benefits from replacing with natural gas.

- US natural gas plants are relatively efficient.
- Methane leakage reduces benefits, depending on efficiency.

Highlights

- CO_2 hydrates were formed in a gas-inducing agitated reactor.
- The changes of CO_2 consumption, induction time, storage capacity etc were observed.
- The effects of gas-inducing stirring, temperature and initial pressure were discussed.
- Induction time was shortened from 261 to 24 minutes with high-speed stirring.

Highlights for review

- An ejector based organic flash combined power and refrigeration cycle is proposed.
- Both 1st and 2nd law analysis conducted.
- Optimum flash pressures exist for maximum 1st and 2nd law efficiencies.
- 1st and 2nd law efficiency improved compared to organic flash power cycle.

Highlights

- The economics of Gulf Stream energy off the North Carolina coast are assessed.
- A portfolio optimization model is developed to identify optimal generation sites.
- The optimal portfolio reduces the variance in monthly electricity generation tenfold.
- The lowest levelized cost for a single 16 MW site can reach 400 $/MWh.
- The lowest levelized cost for an 80 MW portfolio can reach below 300 $/MWh.

Highlights

- City-level environmental efficiency was measured in the Yangtze River Economic Zone during 2003–2014.
- GDP per capita was found acting negatively on environmental efficiency during this period.

- Remote sensing PM2.5 data was incorporated into the undesirable outputs.
- The number of cities below the average environmental efficiency increased from 70 (53.4%) to 83 (63.4%).

Highlights

- Theoretical probability assessment of the pipeline bend failure.
- Maintenance planning based on criteria of avoided risk value and NPV index.
- Assessment of the element failure probability based on microstructure testing.
- Estimation of optimal times to preventive replacement of the steam pipeline.

Highlights

- Transient thermo-hydraulic model for pipeline transportation of natural gas under variable gas quality conditions is proposed.
- Chemical energy flow rate instead of volumetric flow rate is selected as a dependent variable.
- Model validation on field data is carried out.
- Operating strategy of the pipeline system with energy flow rate as a control variable is simulated.
- Advantages of energy-based over volume-based approach are illustrated.

Highlights

- A stochastic expansion planning is addressed on microgrids.
- The planning tool includes two long-term and short-term plans.
- Wind unit, solar panel, energy storage system, and line are installed by plan.
- The planning tool is expressed as a mixed integer nonlinear programming.
- Meta-heuristic optimization algorithm is applied so solve the problem.

Highlights

- We verify the convergence of eco-efficiency through unit root test.
- Eco-efficiency in cement manufacturers converged in the east, middle and west.
- China's cement manufacturers should substitute raw material.

Highlights

- We provide an empirical framework for the efficiency analysis of renewables.
- We find that forecast errors have an impact on the efficiency of allocations.
- We discriminate the empirical results by their time structure.
- We show that renewable infeed has no effect on economic efficiency losses.
- Short gate closures are required for market integration of volatile energy sources.

Highlights

- A feasibility analysis of PV-based hybrid system is carried out.
- HOMER is used to analysed the system sizing.
- Analyses for Cost of Energy, NPC, payback period, and emissions.
- Optimized system is economically feasible compared to SHSs and diesel only systems.
- Proposed system has reasonable environmental benefits and attractive payback period.

Highlights

- Wind/wave climate and energy resources in the Shenzhen coastal zone are studied.
- Monthly, seasonal, and annual wind and wave climate are analyzed and discussed.
- Seasonality in wind power is evident, while spatial fluctuating in the study area.
- The potential of wave energy resources in the Shenzhen coastal zone is limited.

Highlights

- Spin-coating technique are used to construct PBI/GO composite membrane.
- P_{max} of DMAFC and DEAFC obtained at 200 and 120 mW cm^{-2} using Pt-based electrocatalyst.
- Pt-based electrocatalyst is favored for DMAFCs whereas non-Pt is favored for DEAFCs.

Highlights

- Natural-based dye sensitizers extracted and applied in fabrication of DSSCs.
- Dyes were red grape, red onion peel, radish, sour orange peel, and sambucus ebulus.
- Individual, co- and tandem-sensitized configurations are compared for efficiency.
- Highest efficiency was due to red grape and radish in co-DSSC device.
- Tandem was firstly introduced here and resulted in expanded absorption wavelength.

Highlights

- Paper introduces a new parameter “required electric back-up power (P_{rb})” for SBC.
- Analytical model is presented to drive P_{rb}.
- A solar cum electric cooker (SEC) is fabricated as per derived value of P_{rb}.
- Experimental study of SEC verifies the analytical model.

Highlights

- A novel cycle has been proposed for producing water, power and Hydrogen.
- To assess the cycle's performance a model has been developed in EES.
- First and second laws of thermodynamics besides exergoenvironmental analysis have been investigated.
- Imperative system parameters are studied.

Highlights

- Energy flow optimization model put forward to replace technology model.
- Goal programming model was proposed to explain energy flow change.
- Grey correlation degree was used to evaluate the optimization results.
- Method applied in a community heating planning project successfully.
- Scenario planning being enhanced by new models.

Highlights

- We visualize the electrical energy demand in Greece at various time scales.

- We visualize climate-related and socio-economic variables for the same time period.
- We combine the visualizations and compare them to previous relevant studies.
- The results in general confirm the conclusions of previous relevant studies.
- However, some unexpected patterns are revealed.

Highlights

- A new model of solar reactor based on a double-loop fluidized bed has been studied.
- The overall reaction $CO_2 \rightarrow CO + 1/2O_2$ is achieved, by thermochemical cycle.
- The use of nanoparticles as catalyst allows maximizing the surface area of reaction.
- The multi-parameter optimization allowed reaching the mean efficiency of 29.96%, with a maximum of 59.46%.

Highlights

- Three novel models integrated SCWG of coal with power generation are proposed, and analyzed.
- Energetic analyses through energy flow diagrams.
- Maximum thermal efficiency of 46.60% of all the models is obtained.

Highlights

- Different heat transfer types were analyzed in Trombe wall with new channel design.
- Highest amount of convection heat is delivered to the room during sunny period.
- Radiation is the dominant heat transfer process from the Trombe wall.
- Heat transfer is more sensible on the coldest day than the warmest day.

Highlights

- The analysis focuses on six major appliances.
- Econometric models are used to forecast market penetration.
- High-efficiency appliance shares are modeled by logit models.
- Impacts of incentives on energy efficiency improvement are analyzed.
- Annual energy consumption by appliance is evaluated.

Highlights

- Phase diagrams and phase transformation for $LiFePO_4$ synthesis were studied.
- $LiFePO_4$ can decompose to FeP, Fe_2P, and Fe_3P at 718, 776, and 836 °C, respectively.
- Fe_2P formation can be suppressed below temperature 776 °C.
- Excess of Li is beneficial to avoid the formation of Fe_2P.

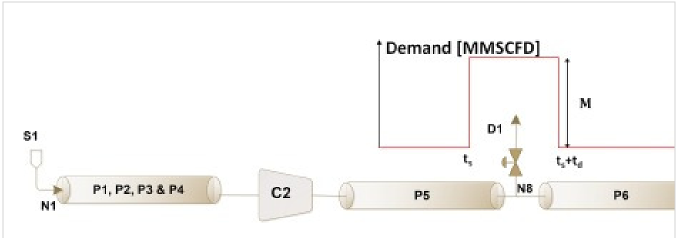

Highlights

- Analyze energy investment decisions that are taken before the uncertainty is revealed.
- Criticism of Monte Carlo simulations to assess behavioral uncertainty.
- Guide to transform a deterministic energy model into a stochastic model.
- No programming of a stochastic solution algorithm is required.

Highlights

- The energy efficiency in Mediterranean countries has been analyzed.
- The two-stage double bootstrap approach has been used.

- The first stage results show the decline of efficiency over the study period.
- Energy efficiency is impacted by different environmental variables.
- Policy recommendations have been provided.

Highlights

- A 1-D mathematical model was developed to evaluate the system performance.
- The evaporative cooling has significant effect on the system performance.
- Wind speed plays a major role in the case of pure forced convection.
- Stable electrical performance for the system while adopting evaporative cooling.
- An optimal value of mass flow rate is found for maximum power output.

Highlights

- Entropy Generation Minimization has been performed for hybrid cycle.
- Novel mathematical modeling of SOFC-ICGT has been proposed.
- A unique performance contour plot for SOFC-ICGT hybrid cycle has been plotted.
- Optimal efficiency of 74.13% has been achieved with entropy minimization of 8.05 W/K.

Highlights

- We examine the impact of financial development on energy consumption in the U.S.
- We provide for breaks and asymmetries in the estimation process.
- The model also include economic growth, trade openness and capital formation.
- Financial development decreases energy demand in the U.S.
- The policy implications of the results are provided.

Highlights

- Systematic framework for Design Operability and Retrofit Analysis (DORA) is proposed.
- DORA analyzes inherent operability and flexibility of an energy system.
- DORA combines operability and flexibility analysis with debottlenecking and retrofitting.

Highlights

- Optimization problems are solved to size and site smart parking lots of electric vehicles.
- The effectiveness of the proposed algorithm is compared to other reported algorithms.
- An adaptive intelligent control strategy with V2G and G2V applicability is proposed.
- A global optimal solution is guaranteed with the proposed model.

Highlights

- This paper presents the failure problems of an integrated energy system.
- Practical engineering problems are investigated and analysed.
- The stochastic behaviours of a limited gas supply are considered.
- The dependencies between the surplus power and the ability of the grid to absorb it is modelled.
- The application of the model is illustrated using an ideal IES.

Highlights

- This work improves the operation of electrical power systems.
- It addresses the design of a convex model for unit commitment.
- The proposed method is based on conic relaxations with valid inequalities.
- The method finds a globally optimal schedule of units in various cases.
- Unlike existing methods, it has a guaranteed efficiency and low complexity.

Waste Heat Recycling

Highlights

- The heat transfer performance in supercritical nitrogen is evaluated.
- The k-ε turbulence model is used in the numerical study.
- Buoyancy causes deterioration at low mass flux and high heat flux conditions.
- The drop in properties triggers deterioration at high mass and high heat flux.

Thermoacoustic micro-electricity generator for rural dwellings in developing countries driven by waste heat from cooking activities Original Research Article
Pages 1107-1120
Kalid O.A. Abdoulla-Latiwish, Xiaoan Mao, Artur J. Jaworski
Abstract | Close research highlights | PDF (3193 K) | View PDF

Highlights

- Demonstrator with just under 20 W of electrical output is modelled and tested.
- Design trade-offs are outlined to apply the technology in poor rural areas.
- Atmospheric air has been shown as a viable thermodynamic medium.
- Use of cheap components has been demonstrated to reduce costs.
- Acoustic and electric efficiencies of 3.5% and 1.9%, respectively, achieved.

Use of pyrolytic gas from waste tire as a fuel: A review Original Research Article
Pages 1121-1131
Dina Czajczyńska, Renata Krzyżyńska, Hussam Jouhara, Nik Spencer
Abstract | Close research highlights | PDF (1375 K) | View PDF

Highlights

- Pyrolytic gas obtained from waste tires is a valuable source of energy.
- Composition and properties of pyrogas varies depending on pyrolysis conditions.
- The special emphasis should be focused on the collection of data on gas emissions.

Biohydrogen production at low load of organic matter by psychrophilic bacteria Original Research Article
Pages 1132-1139
Marcin Zieliński, Ewa Korzeniewska, Zofia Filipkowska, Marcin Dębowski, Monika Harnisz, Rafał Kwiatkowski
Abstract | Close research highlights | PDF (430 K) | View PDF

Highlights

- Psychrophilic bacteria as H_2 producers from organic substrates were investigated.
- The most effective rate of hydrogen production was obtained for *Rahnella aqatilis*.
- Amount of hydrogen production ranged from 16.3 to 58.1 mL/g COD_{fed}.
- *Proteobacteria* may be used as producers of H_2 in psychrophilic conditions.

Articles **1 - 96**

Energy 134 (2017) 24–34

Contents lists available at ScienceDirect

Energy

journal homepage: www.elsevier.com/locate/energy

Optimization of transesterification process for *Ceiba pentandra* oil: A comparative study between kernel-based extreme learning machine and artificial neural networks

F. Kusumo [a], A.S. Silitonga [a, b, c, d, *], H.H. Masjuki [a], Hwai Chyuan Ong [a], J. Siswantoro [e], T.M.I. Mahlia [d]

[a] Department of Mechanical Engineering, Faculty of Engineering, University of Malaya, 50603, Kuala Lumpur, Malaysia
[b] Department of Mechanical Engineering, Politeknik Negeri Medan, 20155, Medan, Indonesia
[c] Department of Mechanical Engineering, Syiah Kuala University, 23111, Banda Aceh, Indonesia
[d] Department of Mechanical Engineering, Faculty of Engineering, Universiti Tenaga Nasional, 43000, Kajang, Selangor, Malaysia
[e] Department of Informatics Engineering, Faculty of Engineering, Universitas Surabaya, Jl. Kali Rungkut, Surabaya, 60293, Indonesia

A R T I C L E I N F O

Article history:
Received 20 May 2016
Received in revised form
29 April 2017
Accepted 31 May 2017
Available online 3 June 2017

Keywords:
Biodiesel
Ceiba pentandra oil
Kernel-based extreme learning machine
Ant colony optimization
Artificial neural network

A B S T R A C T

In this study, kernel-based extreme learning machine (K-ELM) and artificial neural network (ANN) models were developed in order to predict the conditions of an alkaline-catalysed transesterification process. The reliability of these models was assessed and compared based on the coefficient of determination (R^2), root mean squared error (RSME), mean average percent error (MAPE) and relative percent deviation (RPD). The K-ELM model had higher R^2 (0.991) and lower RSME, MAPE and RPD (0.688, 0.388 and 0.380) compared to the ANN model (0.984, 0.913, 0.640 and 0.634). Based on these results, the K-ELM model is a more reliable prediction model and it was integrated with ant colony optimization (ACO) in order to achieve the highest *Ceiba pentandra* methyl ester yield. The optimum molar ratio of methanol to oil, KOH catalyst weight, reaction temperature, reaction time and agitation speed predicted by the K-ELM model integrated with ACO was 10:1, 1 %wt, 60 °C, 108 min and 1100 rpm, respectively. The *Ceiba pentandra* methyl ester yield attained under these optimum conditions was 99.80%. This novel integrated model provides insight on the effect of parameters investigated on the methyl ester yield, which may be useful for industries involved in biodiesel production.

1. Introduction

Biodiesel has gained prominence throughout the world as alternative fuel for diesel engines. Biodiesels as alternative fuels in diesel engines is not new nowadays owing to their favourable physical and chemical properties that are comparable to those for diesel, but with lower engine emissions. There is a growing trend in the biodiesel production capacity not only in developed countries such as France, Germany, Italy and the United States, but also in developing countries such as Brazil, Argentina, Indonesia and Malaysia [1]. The production of alternative fuels from renewable sources have gained much interest from scientists, researchers and industrialists in the field due to concerns on the depletion of fossil fuels and the impact of fossil fuel emissions on the environment. More importantly, there is a critical need to ensure a sustainable supply of energy in order to fulfil the escalating energy demands, which is not possible with fossil fuels since these fuels are derived from non-renewable sources [2]. Concerns over food security have led to the development and enforcement of policies which emphasize the production biofuels from non-agricultural sources [3]. In response to this need, scientists and researchers actively search for ways to produce biodiesels from non-edible feedstocks as well as macroalgae and microalgae [4,5].

Ceiba pentandra (*C. pentandra*) is commonly known as silk-cotton tree. It is a tall plant which belongs to the *Malvaceae* family and it is typically found in tropical rainforests. The seeds of *Ceiba pentandra* contain a relatively high non-edible oil content (~40 %wt, dry basis) and thus, these seeds can be used as potential feedstocks to produce biodiesels. Several experimental have been conducted

* Corresponding author. Department of Mechanical Engineering, Faculty of Engineering, University of Malaya, 50603, Kuala Lumpur, Malaysia.
E-mail addresses: arridina@polmed.ac.id, ardinsu@yahoo.co.id (A.S. Silitonga).

http://dx.doi.org/10.1016/j.energy.2017.05.196
0360-5442/

the production of C. *pentandra* methyl esters (biodiesels) through a conventional process known as alkaline-catalysed transesterification [6,7]. Ong et al. [6] produced C. *pentandra* methyl ester via supercritical transesterification and the process conditions were optimized using response surface methodology (RSM). They achieved a high C. *pentandra* methyl ester yield of 95.5% when the molar ratio of methanol to oil, reaction time, reaction temperature and pressure was 30:1, 476 s, 322 °C and 167 MPa, respectively. Sivakumar et al. [7] used an alkaline-catalysed transesterification process and they also attained a high methyl ester yield of 99.5% using the following molar ratio of methanol to oil of 6:1, KOH catalyst weight of 1 %wt, reaction temperature of 65 °C and reaction time of 45 min.

To date, most of the models used to optimize the process conditions for biodiesel production are based on response surface methodology (RSM) and artificial neural networks (ANN). In both of these approaches, experimental data are used as the groundwork for modelling and optimization [8,9]. However, kernel-based extreme learning machine (K-ELM) models have also been implemented in recent years to study alcoholysis reactions and the process conditions for biodiesel production. Extreme learning machine (ELM) is a learning technique that was initially proposed for generalized single hidden layer feedforward networks (SLFNs) and this technique has been used to optimize processes in various engineering disciplines [10,11]. K-ELM is a learning algorithm used to determine the rational number of hidden neurons in SLFNs based on a kernel matrix. This technique is still rather new, considering that it was developed only in recent years by a few researchers. The main benefit of K-ELM is that the user only needs to identify the necessary parameters and determine one optimum solution using the kernel function. This eliminates the need to specify the number of hidden nodes unlike conventional feedforward neural networks [12,13].

ANN, on the other hand, is fundamentally different from K-ELM since the algorithm is based on the idea that the human nervous system is a data processing system. ANN is widely used for modelling complex phenomena including prediction and classification which involve a large number of independent and dependent [14,15]. Interestingly, ANN is also commonly used to demonstrate the effectiveness of K-ELM models. Ant colony optimization (ACO), however, is an optimization technique that is inspired from observations of the foraging behaviour of ant colonies.

In this study, K-ELM model is developed to predict the process conditions for alkaline-catalysed transesterification of C. *pentandra* oil. Prior to optimization, it is first necessary to develop a reliable prediction model for the transesterification process. There are numerous studies found in the literature pertaining to C. *pentandra* biodiesel production − however, there is a lack of studies pertaining to the mathematical modelling of transesterification process conditions using K-ELM models. In general, the molar ratio of methanol to oil, catalyst weight, reaction time, reaction temperature and agitation speed all play a crucial role in an alkaline-catalysed transesterification process and it is essential to optimize these parameters in order to achieve the highest methyl ester yield and reduce the production costs as much as possible. Hence, in this study, the reliability of the K-ELM and ANN models in predicting the conditions of the alkaline-catalysed transesterification process is determined in order to identify which is the more effective prediction model. The reliability of these models was assessed using the following statistical parameters: coefficient of determination (R^2), mean absolute percent error (MAPE), relative percent deviation (RPD) and root mean squared error (RMSE).

To the best of the authors' knowledge, none of the studies available in the literature have addressed the optimization of process conditions for alkaline-catalysed transesterification of C. *pentandra* methyl ester using a novel, integrated modelling approach, which formed the motivation for this study. Moreover, the best prediction model is chosen for integration with ACO to optimize five conditions of the alkaline-catalysed transesterification process (the molar ratio of methanol to oil, catalyst weight, reaction time, reaction temperature and agitation speed) in order to achieve a high C. *pentandra* methyl ester yield.

2. Materials and methods

2.1. Raw materials and chemical reagents

The crude C. *pentandra* oil chosen for this study, and it was sourced from Koperasi Lestari, Cilacap, Indonesia. The following chemical reagents were all sourced from Merck: analytical-grade methanol with a purity of 99.9%, sulphuric acid with a purity of more than 98.9%, and potassium hydroxide pellets with a purity of 99%. The following certified chemical standards for gas chromatography (GC) were sourced from It Tech Research (M) Sdn Bhd: FAME MIX C8-C24 (100 mg, Supelco-Sigma-Aldrich) and methyl nanodecanoate (C19 with a minimum purity of 99.5%, Supelco-Sigma-Aldrich). Phenolphthalein solution (1% in ethanol) was purchased from Fluka Analytical. Whatman filter papers were sourced from Filter Fioroni, France, each having a diameter of 15 cm.

2.2. Physical and chemical properties

The physical and chemical properties of the crude C. *pentandra* oil and C. *pentandra* methyl ester were determined according to the ASTM D6751 and EN 14214 standards, as shown in Table 4. The physical and chemical properties of biodiesels obtained from other studies are also presented for comparison.

Eq. (1) was used to determine the fatty acid methyl ester (FAME) content in percent (%):

$$FAME = \frac{(\sum A) - A_{EI}}{A_{EI}} \times \frac{C_{EI} \times V_{EI}}{m} \times 100 \quad (1)$$

here, $\sum A$ represents the sum of the peak areas for the FAME, A_{EI} represents the peak area of methyl heptadecanoate, which is the internal standard, C_{EI} represents the concentration of the methyl heptadecanoate solution in heptane (mg/ml), V_{EI} represents the volume of the methyl heptadecanoate solution (ml) and m represents the mass of the methyl ester (mg).

Eq. (2) was used to determine the methyl ester yield in percent (%):

$$Methyl\ ester\ yield = \frac{FAME \times B_{cp}}{O_{cp}} \times 100 \quad (2)$$

here, $FAME$ represents the fatty acid methyl ester content (%), B_{cp} represents the weight of the C. *pentandra* methyl ester (g) and O_{so} represents the weight of the C. *pentandra* oil (g).

2.3. Pre-processing of C. pentandra oil

The crude C. *pentandra* oil needs to be pre-processed prior to transesterification due to its inherent high free fatty acid content, which will lead to saponification and reduce the methyl ester yield. Thus, the crude C. *pentandra* oil was pre-processed by acid-catalysed esterification in the presence of suitable process to reduce the acid value to a lower level (less than 2 mg KOH/g) [6,7]. The acid-catalysed esterification was conducted according to the procedure of Sivakumar et al. [7] using the following parameters: methanol-to-oil volume ratio: 8:1, reaction temperature: 65 °C and H_2SO_4 catalyst weight: 1.834 wt%. The crude C. *pentandra* oil was poured into a three necked flask containing methanol and H_2SO_4 catalyst preheated at 65 °C. The mixture was agitated over a period of 120 min. The temperature was kept at 65 °C throughout the esterification process. On completion of reaction, the mixture was poured into separating funnel and left to stand for several hours. Two layers formed in the separating funnel and the bottom layer was collected in a flask. The extraneous methanol present in the esterified oil was removed by evaporation.

2.4. Alkaline-catalysed transesterification of the esterified C. pentandra oil

The esterified C. *pentandra* oil was poured into a three-necked flask preheated to a temperature range of 40–65 °C using a circulating water bath. Methanol and KOH catalyst were added into the esterified oil and the mixture was stirred on a continuous basis throughout the transesterification process. In this study, the molar ratio of methanol to oil was varied from 3:1 to 15:1 whereas the concentration of the potassium hydroxide (KOH) catalyst was varied from 0.5 to 1.5 %wt The reaction time was varied from 60 to 150 min whereas the agitation speed was varied from 800 to 1200 rpm. Upon completion of the transesterification process, the mixture was transferred into a separating funnel and left to settle until the methyl ester and glycerine were completely separated by gravity. It shall be noted that this separation occurred after 4 h. The top layer is the C. *pentandra* methyl ester whereas the bottom layer is a mixture of glycerine and impurities and therefore, this layer needs to be removed. The C. *pentandra* methyl ester was washed with warm water several times. Lastly, traces of moisture and unreacted methanol were removed using a vacuum evaporator set at 60 °C.

2.5. Design of experiments

The design of experiments (DoE) approach based on the Box-Behnken experimental design was used for modelling and optimization in this study using Design-Expert software version 8.0.3.1 (Stat-Ease Inc., Minneapolis, MN, USA). The designed experiment consists of 46 experimental runs, as shown in Table 1. The molar ratio of methanol to oil (x_1), KOH catalyst weight (x_2), reaction temperature (x_3), reaction time (x_4) and agitation speed (x_5) were varied to achieve the highest C. *pentandra* methyl ester yield (y). Both independent and dependent variables of the designed experiment are presented in Table 1.

2.6. Modelling of the alkaline-catalysed transesterification process

2.6.1. Fundamental concept of ELM

Extreme learning machine (ELM) was initially developed for single-hidden-layer feedforward networks (SLFNs). The parameters in the hidden layer are initialized in a random fashion and the Moore-Penrose generalized inverse is used to compute the output weights. Eq. (3) represents the output function of the ELM for generalized SLFNs [16,17]:

$$f_L(x) = \sum_{i=1}^{L} \beta_i h_i(x) = h(x)\beta \tag{3}$$

In this equation, $\beta = [\beta_1, \cdots, \beta_L]^T$ represents the column vector in which the elements are the output weights between the hidden layer of L nodes and the output node. $h(x)$ represents the output row vector of the hidden layer for each input x, *i.e.* $h(x) = [h_1(x), \ldots, h_L(x)]$. $h(x)$ is used to map the data from the input space of dimension d to the hidden layer feature space of dimension L, H. H is also known as the feature space of the ELM. The training data are given by $\{(x_i, t_i)| x_i \in R^d, t_i \in R^m, i = 1, \ldots, N\}$. The goal of ELM is to attain the smallest training error and the smallest norm of output weights, which is an advantage over other learning algorithms [13,16].

2.6.2. Fundamental concept of K-ELM

If the user has no prior knowledge of the feature space $h(x)$, the user can use Eq. (4) to define the kernel matrix of the ELM [10,18]:

$$\Omega_{ELM} = HH^T \ : \Omega_{ELMi,j} = h(X_i).h(X_j) = K(X_i, X_j) \tag{4}$$

Eq. (5) represents the output function of the ELM classifier:

$$f(x) = h(x)H^T\left(\frac{I}{C} + HH^T\right)^{-1}T = \begin{bmatrix} K(x.x_1) \\ \vdots \\ K(x.x_N) \end{bmatrix}^T \left(\frac{I}{C} + \Omega_{ELM}\right)^{-1} T \tag{5}$$

With this function, it is not essential for the user to have prior knowledge of the feature space $h(x)$. In this case, $h(x)$ corresponds to the kernel $K(u, v)$ (*e.g.* $K(u, v) = \exp(-\gamma u - v^2)$), which is supplied to the user. In addition, it is not essential for the user to know the number of hidden nodes, which is represented by the dimension L of the feature space [12,16]. In this study, MATLAB 7.10.0 software was used to model the alkaline-catalysed transesterification process using K-ELM.

2.6.3. Normalization of the dataset

Normalization was conducted on the dataset for the training model, ensuring that the values are within the range of [0, 1]. Eq. (6) was used for this purpose [12]:

$$N(v) = e_i = \frac{(E_i - E_{min})}{(E_{max} - E_{min})} \tag{6}$$

here, e_i represents and E_i represents the normalized parameter and original parameter, respectively. E_{max} and E_{min} represents the upper and lower bound of the original parameter, respectively.

Once all of the minimum and maximum values were normalized, the predicted values need to be denormalized after the training process. This was done using the inverse of Eq. (5) [12,19].

2.6.4. Hyper parameter tuning

The K-ELM model involves two hyper parameters, namely, the regularization factor (C) and basis function width parameter (γ^2). The best values for these parameters were chosen using the leave-one-out cross-validation (LOOCV) algorithm and the possible values for C and γ were chosen based on the exponent of 2 (*i.e.* 2^{-24}, 2^{-23}, …, 2^{24}, 2^{25}) [12,16].

Table 1
Experiment design matrix for transesterification process.

Parameters	Unit	Coded variables	Coded factor levels		
			1	2	3
Methanol to oil molar ratio	–	x_1	3	9	15
Catalyst concentration	%wt	x_2	0.5	1.0	1.5
Reaction temperature	°C	x_3	50	55	65
Reaction time	min	x_4	60	90	150
Agitation speed	rpm	x_5	800	1000	1200

2.6.5. Random sub-sampling cross validation

The performance of the K-ELM model was assessed using 46 datasets that may not be large enough to evaluate the performance of the K-ELM model. Therefore, random sub-sampling cross validation was used in this study. Random sub-sampling is a multiple holdout which is based on splitting the data randomly into subsets whereby the size of each subset is determined by the user [20,21]. A total of 39 datasets and 7 datasets were used for training and testing, respectively. The procedure was repeated ten times and the average MAPE was determined. Eqs. (6) and (7) was used to determine the standard deviation (SD) and standard error of the mean (SEM), respectively [12]:

$$SD = \sqrt{\frac{\sum_{i=1}^{N}(x_i - \bar{x})^2}{N-1}} \tag{6}$$

$$SEM = \frac{sd}{\sqrt{n}} \tag{7}$$

In Eq. (6), N represents the size of the dataset and $\bar{x}$ represents the mean value of the dataset $x_1, \ldots, x_N$. In Eq. (7), n represents the size of the dataset or the number of observations.

2.6.6. Fundamental concept of ANN

An ANN model was also developed in this study to predict the transesterification process conditions and C. *pentandra* methyl ester yield. MATLAB 7.10.0 software was also used to develop the ANN model. The experimental data, consisting of 46 datasets in total, were divided into training data (80%), cross-validation data (10%) and testing data (10%) in a random manner. The three layer feed-forward scheme was chosen for this study. The *tansig* transfer function was applied for the input layer to the hidden layer while the *purelin* transfer function was applied for the hidden layer to the output layer.

Eqs. (8) and (9) represents the tansig and purelin transfer function, respectively [22,23]:

$$\text{tansig }(x) = \frac{2}{(1 + e^{-2x})} - 1 \tag{8}$$

$$A = \text{purelin }(x) = x \tag{9}$$

The Levenberg-Marquardt backpropagation algorithm was used for the ANN. The ANN architecture is composed of three input layers with five inputs, hidden layers with the optimum number of neurons and one output variable. The five inputs are the molar ratio of methanol to oil, KOH catalyst weight, reaction temperature, reaction time and agitation speed. Training was carried out until the minimum mean squared error (MSE) was reached and the average correlation coefficient (R) was close or equal to 1.

2.6.7. Verification of the data

The following statistical parameters were used to assess the performance of the K-ELM and ANN models: R^2, MAPE, RMSE and RPD. These parameters are given by Eq. (10)–(13) [24,25]:

$$R^2 = 1 - \sum_{i=1}^{n}\left(\frac{(x_{ia} - x_{ib})^2}{(x_m - x_{ib})^2}\right) \tag{10}$$

$$\text{MAPE} = \frac{100}{n}\sum_{i=1}^{n}\left|\frac{x_{ia} - x_{ib}}{x_{ia}}\right| \tag{11}$$

$$\text{RMSE} = \sqrt{\frac{\sum_{i=1}^{n}(x_{ib} - x_{ia})^2}{n}} \tag{12}$$

$$\text{RPD} = \frac{100}{n}\sum_{i=1}^{n}\frac{|(x_{ib} - x_{ia})|}{|(x_{ia})|} \tag{13}$$

here, n represents the number of experimental data. x_{ia}, x_{ib} and x_m represents the experimental value, computed value and mean experimental value, respectively. The R^2 value is an indicator of the accuracy (and hence, reliability) of the prediction models, whereby a higher R^2 value indicates higher accuracy. As a rule of thumb, the R^2 value should be greater than or equal to 80% [26]. The MAPE, RMSE and RPD values indicate the reliability of the model and it is important to reduce these parameters as much as possible.

2.6.8. Sensitivity analysis of the transesterification process conditions

Sensitivity analysis was used to determine the impact of an independent variable towards a dependent variable based on a set of assumptions [27]. Various combinations of inputs were tested using the K-ELM model to determine the impact of each input parameter on the C. *pentandra* methyl ester yield. However, it shall be noted one input was eliminated from each combination. The MAPE was used to assess the impact of each combination of inputs on the predicted C. *pentandra* methyl ester yield using the test dataset.

2.6.9. Optimization of the transesterification process conditions using ACO

ACO is an artificial intelligence technique commonly used to solve complex optimization problems. As the name implies, ACO is inspired from the foraging behaviour of ant colonies [28]. In the wild, ants will leave their nest in search of food and they will leave a chemical scent (known as pheromone) along the way, which is recognized by other members of the colony [19]. Eq. (14) represents the probability of an ant moving from node i to node j [19,29]:

$$P_{i,j} = \frac{\left(\tau_{i,j}^{\alpha}\right)\left(n_{i,j}^{\beta}\right)}{\sum\left(\tau_{i,j}^{\alpha}\right)\left(n_{i,j}^{\beta}\right)} \tag{14}$$

here, $\tau_{i,j}$ represents the amount of pheromone on edge i,j. α represents the parameter used to control the effect of $\tau_{i,j}$. $\tau_{i,j}$ and $n_{i,j}$ represent the desirability of edge i,j (typically $1/d_{i,j}$) whereas β represents the parameter used to control the effect of $n_{i,j}$. Eq. (15) was used to update the amount of pheromone [28,30]:

$$\tau_{i,j} = (1 - \rho)\tau_{i,j} + \Delta\tau_{i,j} \tag{15}$$

In this equation, $\tau_{i,j}$ represents the amount of pheromone on edge i,j, ρ represents the rate of evaporation of the pheromone, and $\Delta\tau_{i,j}$ represents the amount of pheromone deposited.

Eq. (16) was used for the amount of pheromone if ant k travels on edge i,j [29,31]:

$$\Delta\tau_{i,j}^{k} = \begin{cases} \frac{1}{L_k}, & \text{if ant k travels on edge } i,j \\ 0, & \text{Otherwise} \end{cases} \tag{16}$$

Here, L_k represents the cost of the kth ant's tour (typically length) [19,31]. The flow chart of the K-ELM model is shown in Fig. 1.

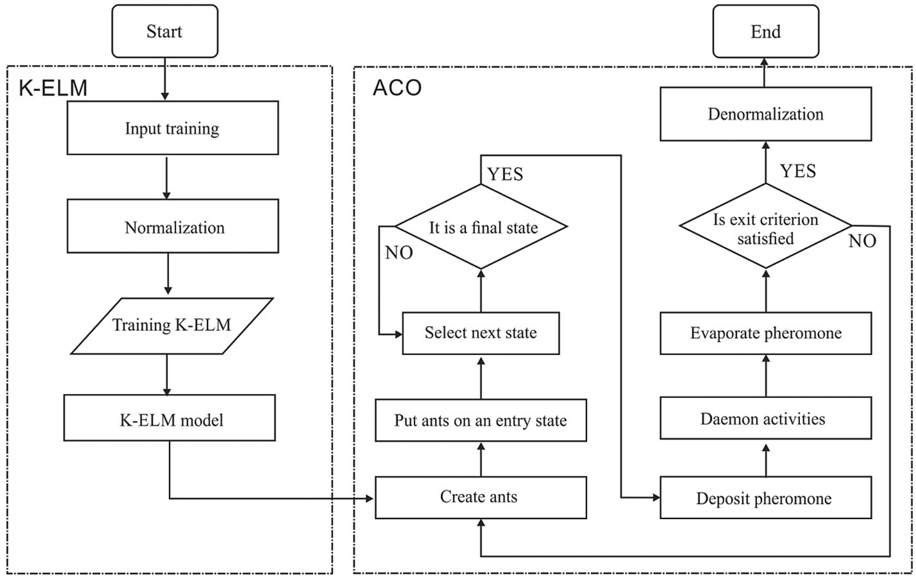

Fig. 1. Flow chart for K-ELM.

3. Results and discussion

3.1. Prediction of the transesterification process conditions by the K-ELM model

The molar ratio of methanol to oil, KOH catalyst weight, reaction temperature, reaction time and agitation speed were used as the inputs in the Box-Behnken designed experimental condition. The aforementioned parameters were optimized in order to achieve the highest C. *pentandra* methyl ester yield. Training was conducted using the K-ELM model until the lowest MSE was achieved and the average R was close or equal to 1. It can be observed from Fig. 2 that R values generated by the K-ELM model from the training value, test value and all value are 0.995, 0.998 and 0.995, respectively. It can be deduced that the model was reliable since the slope of the linear line for the K-ELM model is very close to 1. Hence, the number of iterations was keyed into the programme, initiating training of the data. The training data were compared with the experimental data to verify if the K-ELM model was reliable to predict the conditions of the transesterification process. The R^2, RMSE, MAPE and RPD values were used to assess the reliability of the model [11], as shown in Table 2. It can be seen that the R^2 value of the K-ELM model is 0.991, which was higher than 0.80. The RMSE, MAPE and RPD was found to be 0.668, 0.388 and 0.380 respectively. This indicates that the K-ELM model was reliable as a prediction model because of its high accuracy and low error values. More importantly, the values predicted by the K-ELM model show excellent agreement with the experimental data.

3.2. Random sub-sampling cross validation for the K-ELM model

A total of 39 datasets were used for training whereas the remaining 7 datasets were used for testing. The process was repeated ten times using various combinations of inputs with the same user-defined parameters ($C = 2^{25}$ and $\gamma = 2^0$), as shown in Table 3. Based on the results in Table 3, the SD and MSE of the random sub-sampling cross validation was found to be 0.117 and 0.037, respectively which is indicated the accuracy of the models.

3.3. Prediction of the transesterification process conditions by the ANN model

When implementing ANNs, it was imperative to choose a suitable number of neurons in the hidden layer in order to account for the complexity of the experimental dataset [25,32]. The ANN model was built using a heuristic procedure and the resulting configuration chosen for this study was 5-6-1. This configuration was chosen since it had the lowest MSE for training, validation and testing, with a value of 0.363, 0.596 and 4.331, respectively. This configuration also had the highest R for training, validation and testing, with a value of 0.995, 0.997 and 0.981, respectively. Fig. 3 shows that there is a negligible difference between the testing and validation curves when the ANN was trained for 27 epochs with an error goal of 1×10^{-2}. There is no significant overfitting from the training, validation and testing errors when the number of neurons in the hidden layer was 5, indicating that this number of neurons is suitable for the ANN model. The R^2, RMSE, MAPE and RPD is found to be 0.984, 0.913, 0.640 and 0.643, respectively, as shown in Table 2. It is evident from the residual error of the ANN model that there was good fit between the predicted and experimental data.

3.4. Comparison between the K-ELM and ANN models

The following statistical parameters were used to assess the reliability of the K-ELM and ANN models developed in this study: RMSE, R^2, RPD and MAPE [11,25], and the results are presented in Table 2. The R^2 value for the ANN model and K-ELM model is 0.984 and 0.991, respectively. In general, both of these models are reliable to predict the conditions of the alkaline-catalysed transesterification process. However, the K-ELM model is more accurate than the ANN model, as indicated by the higher R^2 value. The RMSE, RPD and MAPE for the ANN model was 0.913, 0.634 and 0.640, respectively. In contrast, the RMSE, RPD and MAPE are significantly lower for the K-ELM model, with a value of 0.688, 0.380 and 0.388, respectively. The values for each experimental run predicted using the ANN and K-ELM models as well as the corresponding methyl ester yield are shown in Fig. 4. In general, the values predicted by the trained K-ELM model fall within closer proximity of the experimental data compared to the ANN model, implying that the

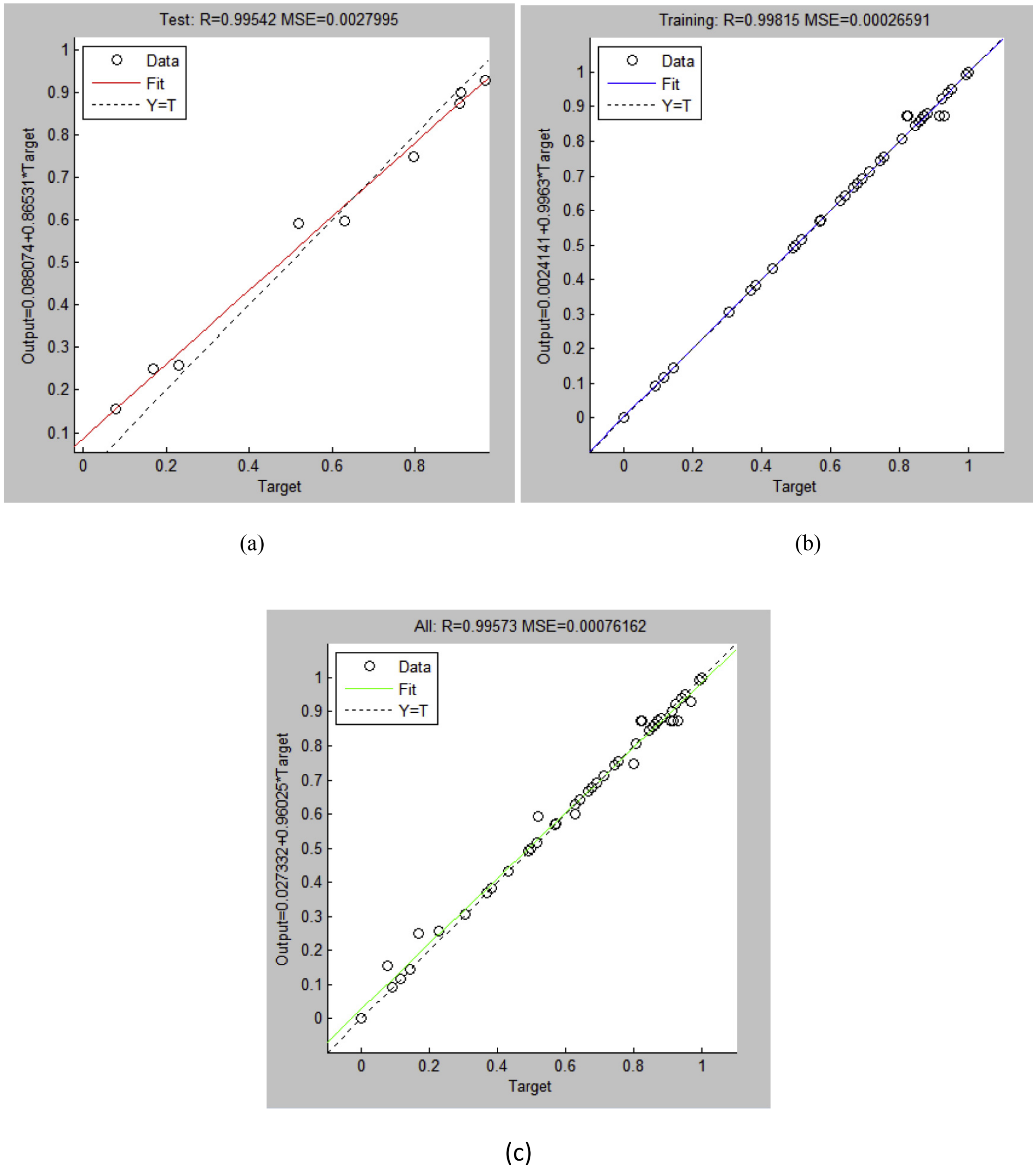

Fig. 2. K-ELM coefficient relation (a) training value and (b) test value and (c) all value.

K-ELM model is more reliable as a prediction model compared to ANN. In addition, the ANN model requires a large number of iterations, which makes it less favourable compared to the K-ELM model [9,33]. For this reason, the K-ELM model was chosen to optimize the transesterification process parameters in order to attain the highest C. *pentandra* methyl ester yield. This was done by integrating the K-ELM model with ACO.

3.5. Sensitivity analysis for the K-ELM model

The MAPE was used to examine the impact of the process conditions on the predicted C. *pentandra* methyl ester yield. Various combinations of inputs were used to determine the impact of each input parameter for the K-ELM model [12,34]. Table 4 shows the impact of different levels of inputs (molar ratio of methanol to oil, KOH catalyst weight, reaction temperature, reaction time and agitation speed) on the C. *pentandra* methyl ester yield based on the MAPE values. The higher MAPE value for the molar ratio of methanol to oil (25.169) indicates that this input variable had a more pronounced impact on the methyl ester yield produced from the transesterification process. Table 4 also shows that the MAPE value for the KOH catalyst weight (5.174) and reaction temperature (5.173) are nearly equal, indicating that these input variables have a similar impact on the methyl ester yield. The MAPE for agitation speed and reaction time was 4.086 and 1.634, respectively. In general, the KOH catalyst weight, reaction temperature and agitation speed somewhat affects the methyl ester yield, though the impact was not as significant as the molar ratio of methanol to oil. The reaction time has the least impact on the methyl ester yield, since this parameter had the lowest MAPE. Hence, the molar ratio of methanol to oil was the most significant parameter for the transesterification process using the K-ELM model.

Table 2
Response for transesterification process.

No	Molar ratio	Reaction Temperature (°C)	Catalyst concentration (%wt)	Reaction time (min)	Agitation speed (rpm)	Methyl ester yield (%)		
						Experiment	ANN	K-ELM
1	3	52.5	0.5	105	1000	76.44	76.11	76.44
2	9	52.5	1.0	105	1000	94.57	95.67	95.75
3	9	52.5	1.0	150	800	93.92	93.51	92.70
4	3	40.0	1.0	105	1000	74.23	73.76	74.23
5	9	65.0	1.0	60	1000	95.36	95.27	95.36
6	15	52.5	0.5	105	1000	81.72	81.83	81.72
7	9	52.5	0.5	60	1000	91.24	91.20	91.24
8	15	52.5	1.5	105	1000	86.92	86.87	86.92
9	9	40.0	1.5	105	1000	90.71	90.74	90.71
10	9	52.5	1.0	105	1000	95.72	95.67	95.75
11	9	52.5	1.5	60	1000	95.51	95.02	95.51
12	15	52.5	1.0	105	1200	89.72	89.77	89.72
13	3	52.5	1.0	150	1000	76.13	76.62	78.04
14	3	52.5	1.0	105	1200	84.86	84.64	84.86
15	9	52.5	0.5	105	1200	97.72	97.70	97.72
16	9	40.0	1.0	60	1000	91.77	91.49	91.77
17	15	52.5	1.0	105	800	83.32	83.22	83.32
18	9	40.0	1.0	105	800	90.06	90.48	90.06
19	9	52.5	1.0	150	1200	98.13	97.86	97.14
20	9	52.5	1.0	60	800	92.58	93.27	92.58
21	3	65.0	1.0	105	1000	79.89	80.03	80.58
22	9	65.0	0.5	105	1000	91.76	92.86	91.76
23	9	65.0	1.0	150	1000	97.01	96.58	97.01
24	9	52.5	0.5	105	800	88.32	87.89	88.32
25	9	40.0	0.5	105	1000	86.52	86.38	86.52
26	3	52.5	1.5	105	1000	77.12	77.07	77.12
27	9	40.0	1.0	150	1000	87.06	86.46	88.84
28	9	52.5	1.5	105	800	94.12	93.59	94.12
29	15	52.5	1.0	60	1000	86.32	82.99	86.32
30	9	65.0	1.5	105	1000	96.72	96.39	96.44
31	3	52.5	1.0	105	800	77.77	77.29	77.77
32	15	52.5	1.0	150	1000	88.28	88.20	88.28
33	3	52.5	1.0	60	1000	78.36	78.34	80.38
34	9	40.0	1.0	105	1200	92.87	93.05	92.87
35	9	52.5	1.0	105	1000	94.52	95.67	95.75
36	9	52.5	1.5	105	1200	97.42	99.41	97.42
37	9	52.5	1.5	150	1000	95.12	94.89	95.12
38	9	52.5	0.5	150	1000	89.76	89.83	88.99
39	9	52.5	1.0	105	1000	97.14	95.67	95.75
40	9	65.0	1.0	105	800	95.98	95.85	95.98
41	9	52.5	1.0	105	1000	96.65	95.67	95.75
42	15	65.0	1.0	105	1000	90.92	88.50	90.92
43	9	52.5	1.0	105	1000	96.82	95.67	95.75
44	9	52.5	1.0	60	1200	98.89	98.12	98.89
45	15	40.0	1.0	105	1000	83.68	81.58	83.68
46	9	65.0	1.0	105	1200	98.69	98.31	98.69
R^2							0.984	0.991
RMSE							0.913	0.688
MAPE							0.640	0.388
RPD							0.634	0.380

Table 3
Random subsampling cross validation.

Repetition	MAPE
Repeat 1	0.723
Repeat 2	0.627
Repeat 3	0.637
Repeat 4	0.416
Repeat 5	0.449
Repeat 6	0.494
Repeat 7	0.581
Repeat 8	0.521
Repeat 9	0.684
Repeat 10	0.380
Overall average	0.551
Standard deviation (SD)	0.117
Standard error of the mean (SEM)	0.037

Table 4
Kernel based extreme learning machine sensitivity analysis.

Parameter removed from the input dataset with five attributes	MAPE
Methanol to molar ratio (X_1)	25.169
Catalyst concentration (X_2)	5.174
Reaction temperature (X_3)	5.173
Agitation speed (X_5)	4.086
Reaction time (X_4)	1.634

3.6. Optimization of the transesterification process conditions using K-ELM model integrated with ACO

As mentioned previously in Section 3.4, the K-ELM model was chosen to be integrated with ACO in order to optimize the molar ratio of methanol to oil, KOH catalyst weight, reaction temperature,

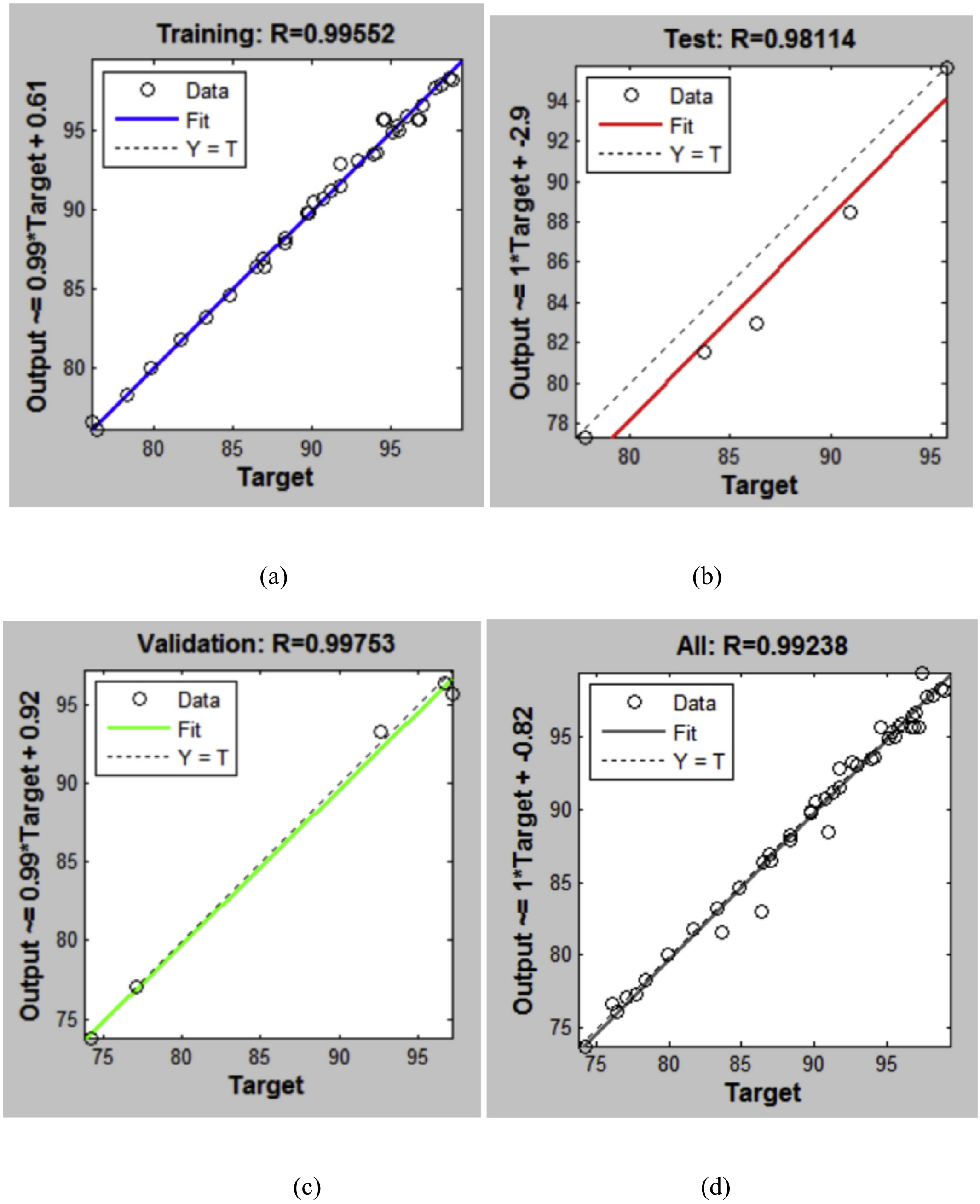

Fig. 3. ANN coefficient relation (a) training, (b) value, (c) validation and (d) all value.

reaction time and agitation speed in order to attain the highest C. *pentandra* methyl ester yield. In order to prove the credibility of the optimization results, the experimental data for the molar ratio of methanol to oil, KOH catalyst weight, reaction temperature, reaction time and agitation speed were keyed in as the inputs for the objective function and the results were compared with the predicted results. The optimum molar ratio of methanol to oil, KOH catalyst weight, reaction temperature, reaction time and agitation speed obtained from the K-ELM model integrated with ACO is 10:1, 1 %wt, 60 °C, 108 min and 1100 rpm, respectively. These are the optimum conditions for the transesterification process based on the optimization model developed in this study. The results are presented in Table 2 and Fig. 5. The C. *pentandra* methyl ester yield predicted with these process conditions is 99.88%, which is in very good agreement with the experimental methyl ester yield, with a value of 99.46%, indicating a minor margin of error. Based on the sensitivity analysis for the K-ELM model, it can be deduced that the methanol-to-oil ratio has the most pronounced impact on the methyl ester yield compared to the other parameters investigated in this study. In general, it can be stated that the K-ELM model integrated with ACO was reliable to optimize the conditions of the transesterification process.

3.7. Physical and chemical properties of the C. pentandra methyl ester

The physical and chemical properties of the C. *pentandra* methyl ester were determined according to the procedure outlined in the

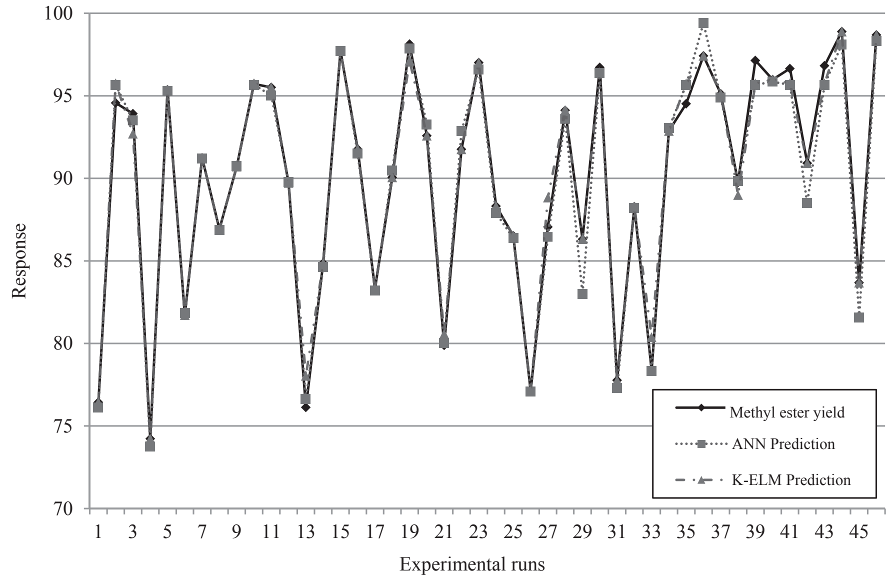

Fig. 4. Comparison between experimental and predicted value.

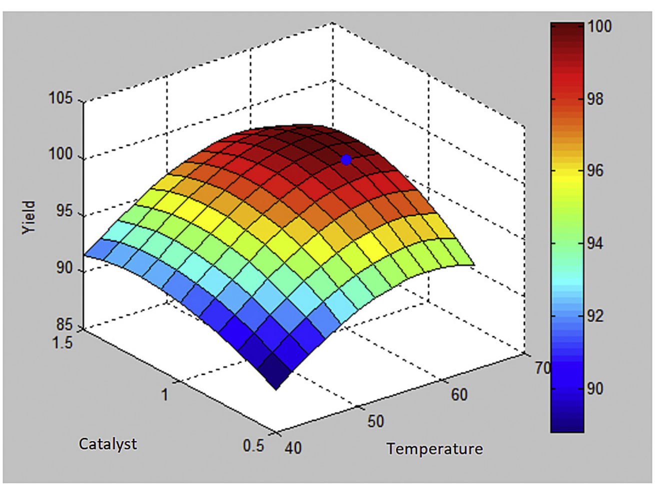

Fig. 5. Optimization of K-ELM model integrated with ACO model at molar ratio of methanol to oil: 10:1, reaction time 108 min and agitation speed 1100 rpm.

ASTM D6751 and EN 14214 standards and the results are presented in Table 5. In general, the physical and chemical properties of the C. *pentandra* methyl ester produced in this study fulfil the biodiesel requirements stipulated in both of these standards. The kinematic viscosity is an important property since it determines the behaviour of the fuel in cold conditions and this property should be between 3.5 and 5 mm^2/s according to ASTM D445 [35]. The density is also an important property of biodiesels besides the kinematic viscosity [36] since it determines the amount of fuel that needs to be injected for a specific engine power. A higher fuel density is undesirable since more fuel needs to be injected into the system at the same engine power. The kinematic viscosity and density of the C. *pentandra* methyl ester produced in this study is 4.69 mm^2/s and 883.6 kg/m^3, respectively. The total acid number is an important property of biodiesels and it is influenced by the free fatty acid composition of the fuel. This property was expressed in milligrams of KOH per gram of sample required to titrate a sample to a specified end point [37]. In general, the total acid number should be as low as possible in order to minimize corrosion of the fuel system and components that are in direct contact with the fuel. The maximum permissible limit for the total acid number according to

Table 5
Physicochemical properties of C. *pentandra* oil and *C.pentandra* methyl ester.

Properties	Unit	Test method	Crude C. *pentandra* oil[a]	C. *pentandra* methyl ester[a]	Kapok methyl ester [7]	Petrol diesel[a]
Density at 15° C	kg/m^3	D 1298	906.5	883.6	875	826
Kinematic viscosity at 40° C	mm^2/s	D 445	18.74	4.69	5.4	2.99
Flash point	°C	D 93	186.5	158.5	156	72.5
Pour point	°C	D 97	–	−2.0	−8	−5
Cloud point	°C	D 2500	–	−3.0	–	−8
Higher heating value	MJ/kg	EN 14214	38.672	40.276	36.292	45.483
Sulphur content	mg/kg	EN ISO 20846	–	8.2	0.5	42.3
Cetane number	–	D 613	–	56.8	54	48.5
Water content	v/v	EN ISO 12937	0.005	0.018	–	0.0015
Copper strip corrosion	–	D 130	–	1a	1a	1a
Oxidation stability	h	EN 14112	–	9.22	–	23.9
Acid number	mg KOH/g	D 664	16.2	0.18	–	0.06
Iodine value	I_2/100 g	EN 14111	116.7	101.5	–	–
FAME	%wt	EN 14103	–	98.9	–	–

[a] Result.

the EN 14104 standard is 0.5 mg KOH/g [38]. The total acid number of the C. *pentandra* methyl ester produced in this study is 0.18 mg KOH/g, which is well below the permissible limit. The flash point of the C. *pentandra* methyl ester is 158.5 °C, which is desirable since the value is higher than that for diesel. The higher flash point of the biodiesel is indeed favourable since it reduces safety hazards when the fuel is stored or shipped to different locations. The cloud point and pour point of the C. *pentandra* methyl ester is −2.0 °C and −3.0 °C, respectively, which are lower than those for diesel. This is indeed expected since the C. *pentandra* oil (the feedstock used to produce the methyl ester) has higher saturated fatty acid content. Copper corrosion strip test was conducted by heating a copper strip to 50 °C in a fuel bath for 3 h. The result shows that the water content of the C. *pentandra* methyl ester was less than 0.05 % vol. It is evident that the physical and chemical properties of the C. *pentandra* biodiesel are superior to those for other fuels, as indicated by the lower kinematic viscosity, higher oxidation stability, higher flash point and higher heating value. In addition, the other physical and chemical properties assessed in this study fulfil the fuel specifications given in the ASTM D6751 and EN 14214 standards, indicating that the *Ceiba pentandra* methyl ester had great potential for use as an alternative fuel for diesel engines.

4. Conclusions

K-ELM and ANN models are developed in this study to predict the conditions of the alkaline-catalysed transesterifcation process for C. *pentandra* methyl ester. The reliability of the K-ELM and ANN models was assessed based on the following statistical parameters: R^2, RMSE, RPD and MAPE. In general, the values predicted by the K-ELM model show excellent agreement with the experimental values, with higher R^2 value and lower RMSE, RPD and MAPE compared with the ANN model. The results prove that the K-ELM model was able to simulate the process conditions of the alkaline-catalysed transesterification in reality with consistent results and reasonable accuracy. In addition, the K-ELM model is more efficient compared to the ANN model since the latter model is more time-intensive to produce the prediction results. Hence, the K-ELM model is chosen to optimize the parameters of the transesterification process, specifically the molar ratio of methanol to oil, KOH catalyst weight, reaction temperature, reaction time and agitation speed in order to attain the highest C. *pentandra* methyl ester yield. This is done by integrating the K-ELM model with ACO. The optimum molar ratio of methanol to oil, KOH catalyst weight, reaction temperature, reaction time and agitation speed which gives the highest methyl ester yield is 10:1, 1 %wt, 60 °C, 108 min and 1100 rpm, respectively. The methyl ester yield predicted with these process conditions is 99.88%, which is in very good agreement with the experimental methyl ester yield, with a value of 99.46%. This shows that the K-ELM model integrated with ACO is a reliable computing tool to optimize the transesterification process conditions in order to maximize the C. *pentandra* methyl ester yield. Even though C. *pentandra* methyl ester is the focus of this investigation, it was believed that this tool will be applicable for other types of biodiesels as well, indicating its adaptability and flexibility. Furthermore, the K-ELM model integrated with ACO can help reduce time, costs and raw materials incurred with conventional trial and error experiments, which is greatly beneficial to industries involved in biodiesel production.

Acknowledgement

The authors wish to acknowledge the Ministry of Education, Malaysia, and University of Malaya, Kuala Lumpur, Malaysia, for funding this work under the SATU Joint Research Scheme (RU021B-2015), PG036-2014B, and Politeknik Negeri Medan, Medan, North Sumatra, Indonesia, under the Research and Community Service Unit (UPPM-2017) and Universiti Tenaga Nasional (Grant No.: 20160101FRGS).

References

[1] Mofijur M, Masjuki HH, Kalam MA, Ashrafur Rahman SM, Mahmudul HM. Energy scenario and biofuel policies and targets in ASEAN countries. Renew Sust Energ Rev 2015;46:51–61.
[2] Dharma S, Ong HC, Masjuki HH, Sebayang AH, Silitonga AS. An overview of engine durability and compatibility using biodiesel–bioethanol–diesel blends in compression-ignition engines. Energ Convers Manage 2016;128:66–81.
[3] Mofijur M, Masjuki HH, Kalam MA, Atabani AE, Shahabuddin M, Palash SM, et al. Effect of biodiesel from various feedstocks on combustion characteristics, engine durability and materials compatibility: a review. Renew Sust Energ Rev 2013;28:441–55.
[4] Nautiyal P, Subramanian KA, Dastidar MG. Production and characterization of biodiesel from algae. Fuel Proces Technol 2014;120:79–88.
[5] Parthiban KS, Perumalsamy M. Nano sized heterogeneous acid catalyst from *Ceiba pentandra* stalks for production of biodiesel using extracted oil from *Ceiba pentandra* seeds. RSC Adv 2015;5:11180–7.
[6] Ong LK, Effendi C, Kurniawan A, Lin CX, Zhao XS, Ismadji S. Optimization of catalyst-free production of biodiesel from *Ceiba pentandra* (kapok) oil with high free fatty acid contents. Energ 2013;57:615–23.
[7] Sivakumar P, Sindhanaiselvan S, Gandhi NN, Devi SS, Renganathan S. Optimization and kinetic studies on biodiesel production from underutilized Ceiba Pentandra oil. Fuel 2013;103:693–8.
[8] Betiku E, Okunsolawo SS, Ajala SO, Odedele OS. Performance evaluation of artificial neural network coupled with generic algorithm and response surface methodology in modeling and optimization of biodiesel production process parameters from shea tree (*Vitellaria paradoxa*) nut butter. Renew Energ 2015;76:408–17.
[9] Prakash Maran J, Priya B. Modeling of ultrasound assisted intensification of biodiesel production from neem (Azadirachta indica) oil using response surface methodology and artificial neural network. Fuel 2015;143:262–7.
[10] Wu S, Wang Y, Cheng S. Extreme learning machine based wind speed estimation and sensorless control for wind turbine power generation system. Neurocomp 2013;102:163–75.
[11] Wong KI, Wong PK, Cheung CS, Vong CM. Modelling of diesel engine performance using advanced machine learning methods under scarce and exponential data set. Appl Soft Comp 2013;13:4428–41.
[12] Wong PK, Wong KI, Vong CM, Cheung CS. Modeling and optimization of biodiesel engine performance using kernel-based extreme learning machine and cuckoo search. Renew Energ 2015;74:640–7.
[13] Zhang L, Yuan J. Fault diagnosis of power Transformers using kernel based extreme learning machine with particle swarm optimization. Appl Math Inf 2015;2:1003–10.
[14] Siswantoro J, Prabuwono AS, Abdullah A, Idrus B. A linear model based on Kalman filter for improving neural network classification performance. Expert Sys Appl 2016;49:112–22.
[15] Sarve AN, Varma MN, Sonawane SS. Response surface optimization and artificial neural network modeling of biodiesel production from crude mahua (*Madhuca indica*) oil under supercritical ethanol conditions using CO_2 as co-solvent. RSC Adv 2015;5:69702–13.
[16] Guang-Bin H, Hongming Z, Xiaojian D, Rui Z. Extreme learning machine for regression and multiclass classification. Syst Cyber Part B IEEE Trans 2012;42:513–29.
[17] Huang G-B, Wang D, Lan Y. Extreme learning machines: a survey. Int J Mach Learn Cyber 2011;2:107–22.
[18] Xu Y, Dai Y, Dong Z, Zhang R, Meng K. Extreme learning machine-based predictor for real-time frequency stability assessment of electric power systems. Neural Comp Appl 2013;22:501–8.
[19] Dorigo M, Gambardella LM. Ant colony system: a cooperative learning approach to the traveling salesman problem. Evol Comp 1997;1:53–66.
[20] Micheline K, Jiawei H, Jian P. Data mining: concepts and techniques. Elsevier.3; 2006. p. 1–740.
[21] Rocha A, Hauagge DC, Wainer J, Goldenstein S. Automatic fruit and vegetable classification from images. Comp Electro Agri 2010;70:96–104.
[22] Rajendra M, Jena PC, Raheman H. Prediction of optimized pretreatment process parameters for biodiesel production using ANN and GA. Fuel 2009;88:868–75.
[23] Garson GD. Interpreting neural-network connection weights. AI Expert 1991;6:46–51.
[24] Lee HV, Yunus R, Juan JC, Taufiq Yap YH. Process optimization design for *jatropha*-based biodiesel production using response surface methodology. Fuel Proces Technol 2011;92:2420–8.
[25] Maran JP, Priya B. Comparison of response surface methodology and artificial neural network approach towards efficient ultrasound-assisted biodiesel production from muskmelon oil. Ultrason Sonochem 2015;23:192–200.
[26] Guan X, Yao H. Optimization of Viscozyme L-assisted extraction of oat bran protein using response surface methodology. Food Chem 2008;106:345–51.
[27] Sarve A, Sonawane SS, Varma MN. Ultrasound assisted biodiesel production

from sesame (*Sesamum indicum* L.) oil using barium hydroxide as a heterogeneous catalyst: comparative assessment of prediction abilities between response surface methodology (RSM) and artificial neural network (ANN). Ultrason Sonochem 2015;26:218–28.
[28] Dorigo M, Maniezzo V, Colorni A. Ant system: optimization by a colony of cooperating agents. Syst Cyber Part B IEEE Trans 1996;26:29–41.
[29] Chandra Mohan B, Baskaran R. A survey: ant colony optimization based recent research and implementation on several engineering domain. Expert Sys Appl 2012;39:4618–27.
[30] Sebayang AH, Masjuki HH, Ong HC, Dharma S, Silitonga AS, Kusumo F, et al. Optimization of bioethanol production from sorghum grains using artificial neural networks integrated with ant colony. Ind Crop Prod 2017;97:146–55.
[31] Boussaïd I, Lepagnot J, Siarry P. A survey on optimization metaheuristics. Info Scie 2013;237:82–117.
[32] Yusaf TF, Yousif BF, Elawad MM. Crude palm oil fuel for diesel-engines: experimental and ANN simulation approaches. Energ 2011;36:4871–8.
[33] Badday AS, Abdullah AZ, Lee K-T. Artificial neural network approach for modeling of ultrasound-assisted transesterification process of crude Jatropha oil catalyzed by heteropolyacid based catalyst. Chem Eng Process Process Inten 2014;75:31–7.
[34] Pal M, Deswal S. Extreme learning machine based modeling of resilient modulus of subgrade soils. Geotech Geol Eng 2014;32:287–96.
[35] Silitonga AS, Masjuki HH, Mahlia TMI, Ong HC, Chong WT, Boosroh MH. Overview properties of biodiesel diesel blends from edible and non-edible feedstock. Renew Sust Energ Rev 2013;22:346–60.
[36] Ong HC, Silitonga AS, Masjuki HH, Mahlia TMI, Chong WT, Boosroh MH. Production and comparative fuel properties of biodiesel from non-edible oils: jatropha curcas, Sterculia foetida and Ceiba pentandra. Energ Convers Manage 2013;73:245–55.
[37] Atabani AE, Silitonga AS, Badruddin IA, Mahlia TMI, Masjuki HH, Mekhilef S. A comprehensive review on biodiesel as an alternative energy resource and its characteristics. Renew Sust Energ Rev 2012;16:2070–93.
[38] Silitonga AS, Masjuki HH, Ong HC, Yusaf T, Kusumo F, TMI Mahlia. Synthesis and optimization of *Hevea brasiliensis* and *Ricinus communis* as feedstock for biodiesel production: a comparative study. Ind Crop Prod 2016;85:274–86.